Annual Report for:

MODELING AND DESIGN FOR REDUCED CROSS TALK IN MIXED SIGNAL ANALOG / DIGITAL IC PACKAGES FOR WIRELESS APPLICATIONS

D. P. Neikirk, Guanghan Xu, and Leszek Demkowicz

The University of Texas at Austin

AFOSR Grant No. F49620-96-1-0032

Grant Start Date: 12/31/95

Report Period: September 1, 1996 - September 1, 1997

POC: Professor Dean P. Neikirk
Department of Electrical and Computer Engineering
The University of Texas at Austin, Austin, TX 78712
voice: 512-471-4669; FAX: 512-471-5445
e-mail: neikirk@mail.utexas.edu; WWW: http://weewave.mer.utexas.edu

Table of Contents

List of Tables

LIST OF FIGURES

Introduction and objectives

A critical requirement for the development of low cost, wide-bandwidth telecommunications equipment is the close integration of both digital and analog microelectronic components. The physical interface between an IC and its environment is the IC package, and its performance is severely tested by the high speed and high frequencies encountered in wide-bandwidth systems. Single chip mixed signal ICs that combine directly both high frequency analog and high speed digital sub-sections will require proper electromagnetic understanding of capacitive, inductive, and radiative coupling between components, and their impact on high sensitivity analog sub-circuits.

The overall objective of this work is the development of techniques for the analysis and design of mixed signal packages, especially the impact of inductive cross talk between the digital and analog sections of the IC, and techniques to maintain appropriate RF to RF signal line isolation in low cost IC packages. In wireless personal communication services (PCS) units there are particularly severe constraints on package options, since these applications are typically very cost and form-factor sensitive. Some of the major problems induced by digital to analog and analog to analog cross talk are listed below:

(1) high speed digital clocks cause severe interference with RF or IF front ends;
(2) in digital portables, time-division-multiple-access (TDMA) may be used and power on / off cycles happen fairly frequently, causing additional transient noise on the power and ground planes;
(3) in frequency division duplex systems, high-power transmit signals cause interference with weak receive signals since separation by filters is limited;
(4) the leakage of the amplifier output to the input may cause the amplifier to oscillate.

Under this program, we are developing and testing electromagnetic modeling techniques that can capture such effects; to achieve this it is critical that the electromagnetic analysis tools *exclude* unnecessary effects, but without requiring "expert" intervention. We are developing inductive extraction processes that use ultra-compact equivalent circuits (consisting of frequency-independent elements) to model frequency dependent skin and proximity effects. Recent accomplishments include a new highly efficient simulation method, the surface ribbon method (SRM), that allows much more rapid simulation to be performed. Typically, computation time can be reduced by about a factor of 2000 compared the conventional model. We are currently preparing user software for transmission line impedance modeling based on the SRM, and expect release in first quarter 1997. We have recently derived a rigorous definition for the “effective internal impedance” used with the surface ribbon method, and will begin investigating its use with the finite element method. This approach should allow significant improvement in computation time for FEM-based electromagnetic simulations of finite conductivity structures. We are also studying internal-to-the-package low pass filter designs for analog power supply to chip; pad / pin arrangements for reduced digital power plane-to-analog coupling, for RF controlled impedance connections, and for increased RF-to-RF signal line isolation. Prototypical wireless communications circuits will be used to determine the impact of digital-to analog interference, and validate the models developed.

ACCOMPLISHMENTS FOR THIS REPORTING PERIOD (9/1/96 - 9/1/97)

EFFECTIVE INTERNAL IMPEDANCE BOUNDARY CONDITION FOR FINITE CONDUCTIVTY METALS

Impedance boundary conditions (IBCs) are widely used in scattering problems, eddy current problems, and lossy transmission line problems. An IBC is usually adopted to simplify the problems by eliminating from the domain to be solved, for example, lossy dielectrics, multi-layered coatings on conductors in scattering problems, or the lossy conductors in eddy current and transmission line problems. Solutions can then be obtained by applying the finite element method (FEM) [1, 2], the boundary element method (BEM) [3, 4], the electric/magnetic field integral method (MFIE/EFIE) [5, 6], the finite difference time domain method (FDTD) [7, 8], etc.. In each case, the use of an IBC reduces the number of unknowns and can substantially reduce the computation time required. But, in

general, the boundary condition must be known (at least approximately) *a priori* on the surface, and the accuracy of the field solution is determined by the accuracy with which the IBC is approximated.

The most widely used IBC is the standard impedance boundary condition (SIBC), also called the Leontovich boundary condition [9, 10], that was originally developed for use when the skin depth is small relative to other dimensions of the problem, or a layer is thin and highly lossy. In general, for coated dielectric layers on scatterers, the reflection of the electromagnetic wave at the boundary depends on the angle of the incident wave, and hence requires higher level of IBCs [10], such as the Tensor Impedance Boundary Condition (TIBC), the Higher Order Impedance Boundary Conditions (HOIBC), etc. For eddy current and transmission line problems, the Leontovich boundary condition has been used to model lossy conductors at high frequency. In this paper, an efficient approach for calculating the series impedance of lossy multi-conductor lines from DC to high frequency is presented that use the effective internal impedance (EII) as an impedance boundary condition. The advantage of the EII when compared to the SIBC is that even for strongly coupled transmission lines it is easily approximated from low frequency (i.e., the skin depth is larger than the cross-sectional dimensions of the conductors) to high frequency (i.e., the skin depth is far smaller than the dimensions of the conductors) using the surface impedance of an isolated conductor. As an example, the EII-based method and the SIBC combined with the BEM are compared in the case of twin lead conductors, and the appropriateness of the EII approach is shown for series impedance calculations of lossy quasi-TEM transmission lines from DC to high frequency.

Schelkunoff [11] first introduced the concept of surface impedance in electromagnetics in 1934 for the analysis of coaxial cables. In the 1940's Leontovich [9] as well as many other workers studied the basic properties of the surface impedance for a semi-infinite plane of an isotropic linear medium and on a conductor-backed thin lossy dielectric layer where a plane wave is incident. Senior [12] explained in detail the Leontovich boundary conditions and the requisites to be satisfied. According to Leontovich, at the surface of the lossy conductor the electric and magnetic fields are related by

$$\vec{E} - (\hat{n} \cdot \vec{E})\hat{n} = Z_s \hat{n} \times \vec{H} \quad , \tag{1}$$

where $\vec{E}$ is the electric field, $\vec{H}$ is the magnetic field, Z_s is the surface impedance, and $\hat{n}$ is normal outward unit vector. For a semi-infinite thickness plane of an isotropic linear lossy conductor, the surface impedance is given by

$$Z_s(\omega) = \sqrt{\frac{j\omega\mu}{\sigma}} = \frac{(1+j)}{\sigma\delta} \quad , \tag{2}$$

where ω is the frequency in radians per second, μ the permeability, σ the conductivity, and δ the skin depth. For a thin lossy dielectric with permittivity ε and conductivity σ backed by a perfect conductor, the surface impedance is

$$Z_s(\omega) = \sqrt{\frac{j\omega\mu}{\sigma + j\omega\varepsilon}} \tanh\{\gamma(\omega)d\} \quad , \tag{3}$$

where the propagation constant in the dielectric is $\gamma(\omega) = \sqrt{j\omega\mu(\sigma + j\omega\varepsilon)}$ and d is the thickness of the dielectric layer.

In order to use (2) or (3) to approximate the SIBC for multi-conductor problems the relationship between the tangential electric and magnetic fields at any point on the boundary must be (at least approximately) a local one, depending only on the curvature of the surface and the local electromagnetic properties (i.e., μ, ε, and σ) of the bodies. Hence, to use the simple expressions given by (2) or (3), the surface impedance must not be altered by the global geometry of the conductor or the existence of other conductors in a problem. This constraint will hold if the operating frequency is "high" (but much lower than the dielectric relaxation frequency), i.e., when the curvature radius of the surface is larger than the skin depth, when the refractive index of the bodies is larger than that of the external medium, and when the dimensions of the problem are smaller than the wavelength. In such circumstances, the reflection characteristic is independent of the incident angle. For geometries

having curvature, Leontovich introduced a first order curvature correction term to the surface impedance for small radii of curvature and Mitzner [13] later refined this.

At low and middle frequency where the skin depth is comparable to or larger than the dimensions of the conductors, the surface impedance is strictly no longer a local property and depends on the global geometries of the conductors. For "thin-film" transmission lines using metals with thicknesses of less than a few micrometers, such a condition may hold for frequencies well into the GHz range. Under such conditions the surface impedance when other conductors are present may considerably differ from the surface impedance of an isolated conductor. Hence, it is difficult to know or approximate *a priori* the surface impedance in lossy multi-conductor systems at low to middle frequencies. This limits the usefulness of the SIBC for calculating the series impedance of lossy quasi-TEM transmission lines at low and middle frequencies, and necessitates complicated models for the IBC.

It would be useful to find some technique in which surface characteristics can be more easily approximated than the standard surface impedance boundary condition. Instead of developing complicated SIBC models to capture the coupling and non-localized field effects between multiple conductors at low and middle frequency it is possible to develop a formulation in which *isolated* conductor surface impedance is a useful approximation. In this approach, the conductor interior is <u>not</u> excluded from the domain of solution, but rather the conductor interior is replaced by the exterior medium and the Green's function of the exterior medium is used also for the interior region in the equivalent problem. The conductor is now modeled as an impedance sheet at the conductor surface, as shown in Fig. 1b, the electric field is assumed continuous across the surface of conductor, and a sheet current is assumed at the surface of conductor.

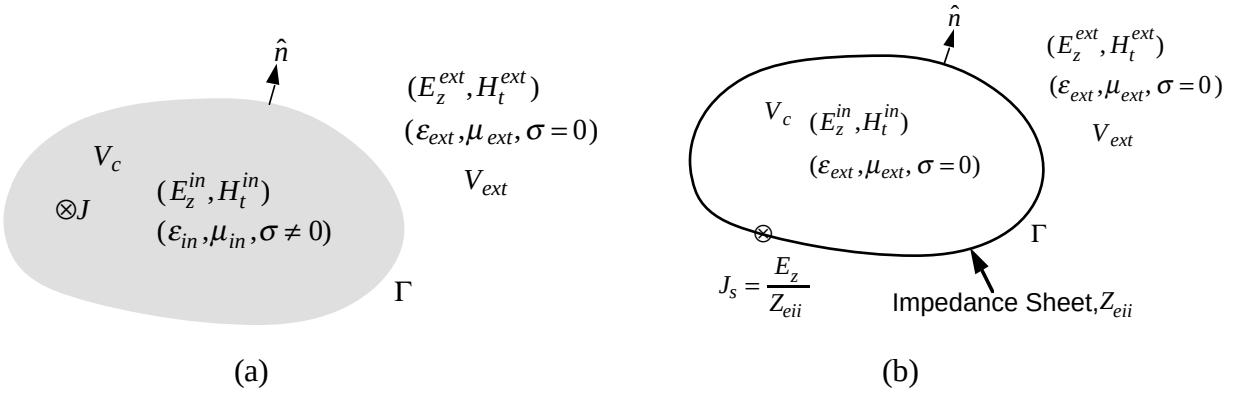

Figure 1: Comparison of the actual geometry and various surface equivalent models.
(a) actual geometry with the descriptions of fields and material properties; (b) the equivalent model using the effective internal impedance (EII) where the exterior fields are identical to the original problem, the conductor interior is replaced by the exterior medium, and an impedance sheet is defined at the conductor surface.

For the exterior region the boundary integral equation becomes

$$\sum_{q=1}^{m} \oint_{\Gamma_q} dr' G_{ext}^1(r,r') j\omega\mu H_t^{ext}(r') - \sum_{q=1}^{m} \oint_{\Gamma_q} dr' \left[G_{ext}^2(r,r') - 0.5\delta(r-r') \right] \cdot \left(E_z(r') + \nabla_z \Phi^q \right) = 0 \quad , \tag{4}$$

where H_t^{ext} is the exterior magnetic field and E_z is the electric field at the conductor perimeter Γ_q. For the interior region in the equivalent problem, the boundary integral equation becomes

$$\oint_{\Gamma_q} dr' G_q^1(r,r') j\omega\mu H_t^{in}(r') - \oint_{\Gamma_q} dr' \left[G_q^2(r,r') + 0.5\delta(r-r') \right] E_z(r') = 0 \quad , \tag{5}$$

where H_t^{in} is the interior magnetic field in the equivalent problem, and the Green's function of the exterior medium is used instead of the Green's function of the conductor.

For this new equivalent problem the relationship between the tangential electric field and the difference of the tangential magnetic fields across the impedance sheet is called the effective internal impedance (the EII, to distinguish it from the SIBC), and is then

$$Z_{eii}(\omega, r') = \frac{E_z(r')}{H_t^{ext}(r') - H_t^{in}(r')} = \frac{E_z(r')}{J_s(r')} \quad , \tag{6}$$

where Z_{eii} is the EII. If H_t^{ext} and E_z in (6) are set to the exact (i.e., identical to those in the original problem) external magnetic and electric fields and H_t^{in} in the EII problem is calculated from (5) (again using the exact electric field from the original problem), then an "exact" EII can be *a posterior* determined. This EII is consistent with (i.e., given the correct EII, it can be used to calculate) the exterior magnetic and electric fields of the original problem. The EII does, however, produce a finite interior magnetic field in the equivalent problem, unlike the "null" interior magnetic field obtained using the SIBC and the BEM.

To complete the statement of the EII formulation, power applied, power dissipated, and magnetic energy stored in the equivalent problem are found using

$$-\int_S ds \nabla \Phi^q \cdot \vec{J}_s^* = \int_S ds Z_{eii} |J_s|^2 + j\omega \int_S ds \vec{A} \cdot \vec{J}_s^* \quad . \tag{7}$$

Resistance can be calculated using

$$R_q^{eii}(\omega) = \frac{\oint_{\Gamma_q} dr' \mathbf{Re}\left\{ Z_{eii} |J_s|^2 \right\}}{\left| \oint_{\Gamma_q} dr' J_s \right|^2} \cdot l_q \quad . \tag{8}$$

Internal inductance of conductor q and total external inductance are calculated using

$$L_{in,q}^{eii}(\omega) = \frac{\mu \int_{V_q} dv \vec{H}^{in} \cdot \vec{H}^{in*}}{|I_q|^2} = -\frac{\int_{S_q} ds \hat{n} \cdot \left(\vec{A} \times \vec{H}^{in*} \right)}{\left| \oint_{\Gamma_q} dr' J_s \right|^2}$$

$$= -\frac{\oint_{\Gamma_q} dr' \mathrm{Im}\left\{ E_z H_t^{in*} \right\}}{\omega \left| \oint_{\Gamma_q} dr' J_s \right|^2} \cdot l_q \tag{9}$$

and

$$L_{ext}^{eii}(\omega) = \frac{\mu \int_{V_{ext}} dv \vec{H}^{ext} \cdot \vec{H}^{ext*}}{\sum_{q=1}^{m} |I_q|^2} = \frac{\int_S ds \hat{n} \cdot \left(\vec{A} \times \vec{H}^{ext*} \right)}{\sum_{q=1}^{m} \left| \oint_{\Gamma_q} dr' J_s \right|^2}$$

$$= \sum_{q=1}^{m} \left(\frac{\oint_{\Gamma_q} dr' \, \mathrm{Im}\left\{ \left(E_z + \nabla \Phi^q \right) H_t^{ext*} \right\}}{\omega \left| \oint_{\Gamma_q} dr' J_s \right|^2} \right) \cdot l_q \quad . \tag{10}$$

Surface inductance due to the magnetic energy stored at the impedance sheet is given by

$$L_{sur,q}^{eii}(\omega) = \frac{\int_S ds \, \mathbf{Im}\left\{ Z_{eii}^q \left| J_s \right|^2 \right\}}{\omega \left| I_q \right|^2} = \frac{\oint_{\Gamma_q} dr' \, \mathbf{Im}\left\{ Z_{eii}^q \left| J_s \right|^2 \right\}}{\omega \left| \oint_{\Gamma_q} dr' J_s \right|^2} \cdot l_q \quad . \tag{11}$$

Finally, the sum of internal, external, and surface inductances from (9), (10), and (11) gives the total series inductance for the transmission line in the EII formulation. Using the exact exterior magnetic and electric fields from the original problem the resistances in the original and EII problems are identical), as are the "external" and "internal" inductances.

The following integral equation can be formulated using the EII

$$\sum_{q=1}^{m} \oint_{\Gamma_q} dr' \left\{ j\omega\mu G_{ext}^1 + \delta(r - r') Z_{eii}(r') \right\} J_s(r') + \sum_{q=1}^{m} \oint_{\Gamma_q} dr' \delta(r - r') \nabla_z \Phi^q = 0 \quad . \tag{12}$$

Each conductor perimeter Γ_q can be further broken into N_q segments $C_{q,i}$, where these pieces represent current-carrying "ribbons" of width w_i. Equation (26) then becomes

$$Z_{eii}^{m,k}(r) J_s^{m,k}(r) + j\omega\mu \sum_{q=1}^{m} \sum_{i=1}^{N_q} \int_{C_{q,i}} dr' \, J_s^{q,i}(r') G_{ext}^1(r, r') = -\nabla_z \Phi^m, \tag{13}$$

where $Z_{eii}^{m,k}$ and $J_s^{m,k}$ are the effective internal impedance and sheet current density on the k[th] ribbon of the m[th] conductor at a given frequency, and the second term of the left hand side represents contributions from self and mutual inductances. If the ribbons are narrow enough that the sheet current density is constant across each ribbon, integrating over the k[th] ribbon yields

$$\frac{I_s^k}{w_k} \int_{C_k} dr \left(Z_{eii}^k(r) \right) + j\omega\mu \sum_{i=1}^{N} \frac{I_s^i}{w_i} \int_{C_k} \int_{C_i} dr' \, dr G_{ext}^1(r, r') = - \int_{C_k} dr \nabla \Phi^k \quad , \tag{14}$$

where I_s^k is the total sheet current carried by the k[th] ribbon and $N = N_q \times m$. Finally,

$$\overline{Z_{eii}^k} \, I_s^k \frac{l_k}{w_k} + j\omega\mu \sum_{i=1}^{N} \frac{I_s^i \, l_k}{w_k \, w_i} \int_{C_k} \int_{C_i} dr' dr G_{ext}^1(r, r') = \Phi_1^k - \Phi_2^k \quad , \tag{15}$$

where $\Phi_1^k - \Phi_2^k$ is voltage drop along ribbon k, $\overline{Z_{eii}^k}$ is the EII averaged over the width of ribbon k, and l_k is the length of ribbon k. Equation (29) can be expressed as an N x N matrix equation

$$\left[\left[Z_{eii} \right] + j\omega [L] \right] [I] = [V] \quad , \tag{16}$$

where $[Z_{eii}]$ is an N x N diagonal matrix made up of the $\overline{Z_{eii}^k}$'s. This approach is called the surface ribbon method (SRM) [14-16]. One advantage of the SRM is that the number of ribbons that is required on each conductor can be quite small while still yielding accurate results [16]. A similar approach was used in [17] for transient analysis of multi-conductor transmission lines, although only a simple resistance was used for the internal impedance of the conductors.

Just as in the SBEM, in principle it is as difficult to find *a priori* the exact EII, especially at low and middle frequencies, as solving the original problem. However, it will be shown below that the surface impedance of a single, isolated conductor is a better approximation to the EII than to the SIBC for multi-conductor transmission lines at low frequencies, while at high frequencies the isolated conductor surface impedance is an adequate approximation of both the EII and the SIBC. Hence, more accurate approximation of the transmission line series impedance can be obtained over a wider frequency range using the more easily calculated isolated conductor surface impedance as an EII in the SRM than can be achieved using the same isolated surface impedance as the SIBC in, for instance, the SBEM.

Example: Circular Cylindrical Conductors (Twin-lead)

A simple test case for the EII in the SRM is closely coupled, parallel circular wires, or "twin lead" transmission line. For the two-dimensional geometry shown in Fig. 2, the "full" (i.e., full solution both exterior and interior to the conductors) BEM (FBEM), the BEM using the surface impedance of an isolated conductor as an approximation for the SIBC (I-SBEM), and the SRM using the surface impedance of an isolated conductor as an approximation for the EII (I-SRM), have been applied to calculate the series resistance and inductance of twin lead. The surface impedance of an isolated circular wire used in the I-SBEM and I-SRM is found by solving the Helmholtz equation for the cylindrically-symmetric conductor, giving

$$Z_s = \frac{j\sqrt{j\omega\mu\sigma}}{\sigma}\frac{J_0\left(jr\sqrt{j\omega\mu\sigma}\right)}{J_1\left(jr\sqrt{j\omega\mu\sigma}\right)} \quad , \tag{17}$$

where r is the radius of the circular conductor, and J_0 and J_1 are Bessel functions of the first kind [18].

The most challenging test case is for closely spaced twin lead. For a gap between the outer surfaces of the two conductors equal to 20% of the wire radius, Fig. 3 compares the exact SIBC (found *a posterior* using the exact fields found from the full BEM solution), the exact EII (found *a posterior* using the exact fields), and the surface impedance of an isolated conductor. Close agreement between the EII or the SIBC and the isolated conductor surface impedance is an indication that using (17) as an approximation should lead to a good approximation for the series impedance per unit length for the twin lead. At low frequency (i.e., ω such that $\delta = 2r$), the EII for the twin lead is quite close to the surface impedance of an isolated conductor, while the SIBC for the twin lead is not; hence we expect the I-SRM to yield a good approximation for the low frequency impedance, while the I-BEM should produce a larger error. At high frequency (i.e., $\delta = \frac{0.2}{3}r$), both the EII and the SIBC of the twin lead converges to the surface impedance of an isolated conductor (which itself approaches $\frac{(1+j)}{\sigma\delta}$ at high frequency), although the EII approaches this limit more slowly than the SIBC. This indicates that both the EII and the SIBC will yield a good approximation to the series impedance at high frequency. Over a narrow band of frequencies in the middle frequency range (i.e., when the skin depth is approximately equal to the wire radius) neither the EII nor the SIBC are well approximated by the isolated conductor surface impedance, although the average value over the surface is approximately the same as the isolated conductor value.

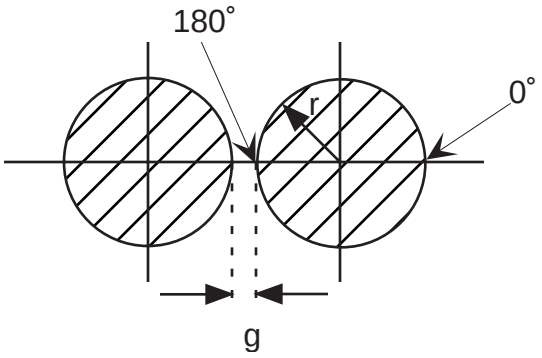

Figure 2: Geometry of twin lead used to test the EII the SRM.
0˚ corresponds to the "outside" point on the surface, and 180˚ corresponds to the inside face.

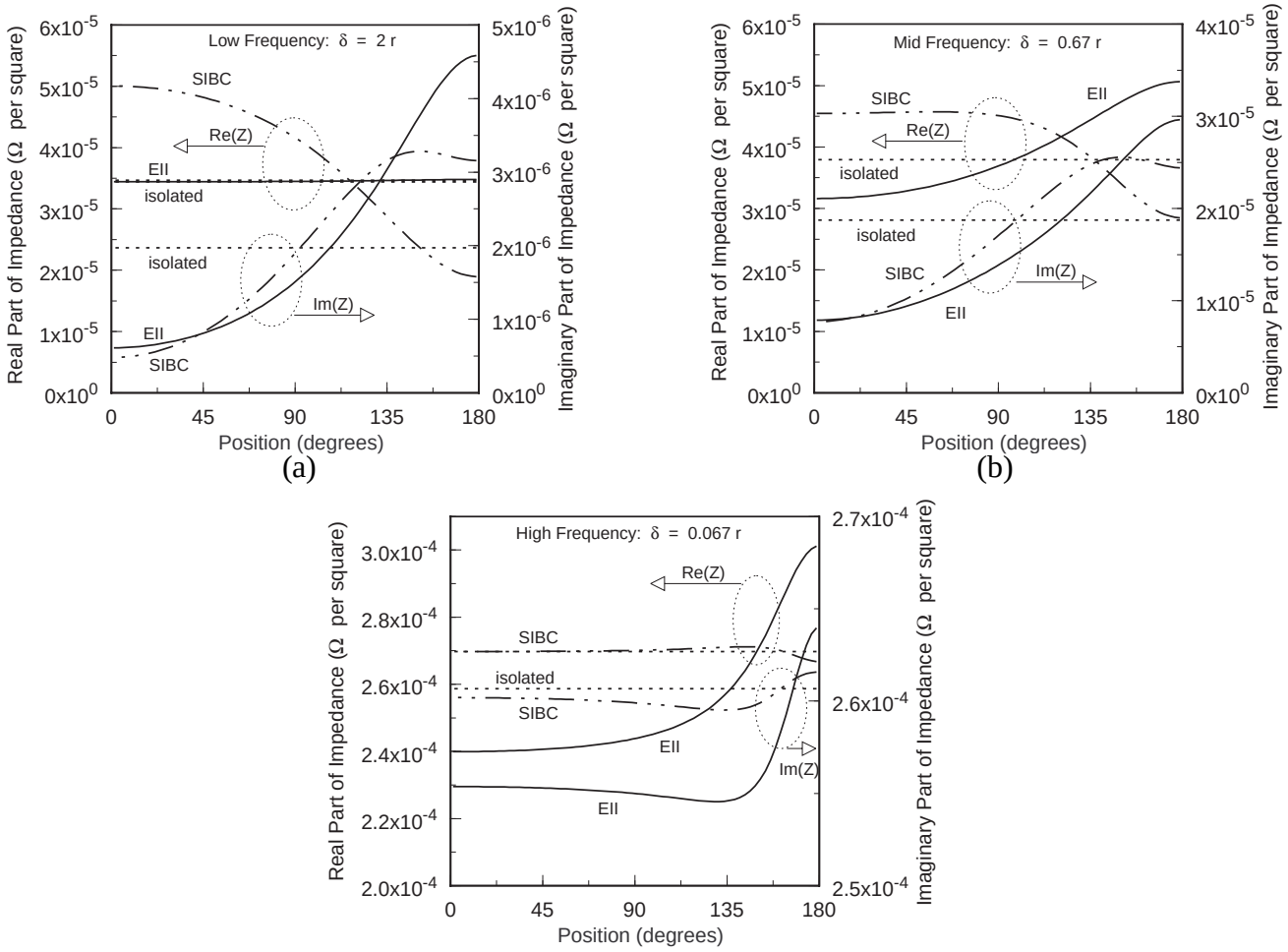

Figure 3**:** Comparison of the SIBC, the surface impedance of an isolated conductor, and the EII for twin lead.
Radius is 1 mm, separation of 0.2 mm, using conductors with $\sigma = 5.8\text{x}10^7$ S m^{-1}, as a function of position on the conductor surface. Dashed line (▮▮▮▮▮▮▮▮▮▮▮▮▮▮▮▮▮): isolated conductor surface impedance (from (32)); solid line (▬▬▬▬▬▬▬▬▬▬▬▬▬▬▬▬▬): the EII; dot-dashed line (▬ ▮ ▬ ▮ ▬): the SIBC. (a) Low frequency comparison at $\delta = 2r$; (b) middle frequency comparison at $\delta = \frac{2}{3}r$; (c) high frequency comparison at $\delta = \frac{0.2}{3}r$.

Figure 4 shows the series impedance calculated using the FBEM, I-SBEM, and I-SRM for closely spaced twin lead. If the exact surface impedance (rather than the isolated) is used as the SIBC

in the SBEM or the exact EII is used in the SRM, the surface techniques give identical external fields and series impedance to full BEM over the entire frequency range. Using the isolated conductor surface impedance as an approximation for the SIBC and EII, the calculated low frequency resistances per unit length are almost all identical to the DC resistance of the twin lead, regardless of technique. Resistances calculated using I-SBEM and I-SRM deviate from the exact resistance (from the FBEM calculation) by 12% and 7%, respectively, at middle frequency, and 4% at high frequency. At both high and low frequency the inductance calculated using the I-SRM is very close to the inductance found using the FBEM. The largest error in the I-SRM calculation occurs at middle frequencies, although the error is at worst 6%. The I-SBEM overestimates the inductance at low frequency by about 17%, again as expected since the correct SIBC at low frequency is significantly different from the isolated surface impedance. At middle and high frequencies the I-SBEM is almost identical to the FBEM calculation.

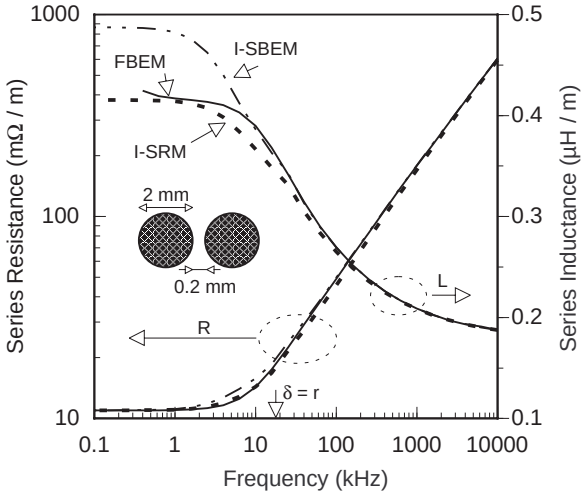

Figure 4**:** Comparison of resistance and inductance calculated using various techniques.
Twin lead is closely coupled: 1 mm radius, 0.2 mm spacing, and $\sigma = 5.8 \times 10^7 S \cdot m^{-1}$ (copper). Solid line (▬▬▬▬▬▬): full boundary element method (FBEM) solution; dot-dashed line (▬ ▮ ▮ ▬ ▮ ▮ ▬): surface boundary element method using the surface impedance of an isolated conductor as an approximation for the SIBC (I-SBEM); Dashed line (▮▮▮▮▮▮▮▮▮▮▮▮▮▮▮▮): surface ribbon method using the surface impedance of an isolated conductor as an approximation for the EII (I-SRM).

Table 1 compares the number of unknowns and run time on an IBM RISC 6000 for the FBEM, the I-BEM, and the I-SRM. The surface techniques are at least 25 times faster than the FBEM in assembling the required matrices, and at least 11 times faster in solving using a gaussian elimination algorithm. In addition, the SRM and the SBEM require matrix assembly only once for all frequencies of interest, while FBEM requires assembling the matrix at each frequency. Hence, the surface techniques are significantly more computationally efficient, and by using the isolated conductor surface impedance as an approximation for the EII in the SRM, little accuracy is lost over the whole low-to-high frequency range.

Method	Number of unknowns	CPU time (sec) Assembling	Solving
BEM	578	468.1	100.10
I-SBEM	290	18.3	8.05
I-SRM	287	5.1	8.96

Table 1: Run time comparison between BEM and SRM.
Comparison of run time on an IBM RISC 6000 for BEM, BEM assuming the SIBC is equal to the isolated conductor surface impedance (I-SBEM), and SRM assuming the EII is equal to the isolated conductor surface impedance (I-SRM). The surface of a conductor is segmented into 144 elements. I-SBEM and I-SRM are at least 25 times faster than BEM in assembling a matrix, and at least 11 times in solving the matrix using a simple gaussian elimination algorithm.

In summary, this work has shown a new surface impedance technique that can be accurately approximated using the isolated conductor surface impedance, even at low frequency. This effective internal impedance (EII) can be combined with the surface ribbon method (SRM) allowing numerically efficient and accurate calculation of the series impedance of lossy multi-conductor transmission lines. In this technique, the effective internal impedance defines an impedance sheet at the conductor surfaces and the conductor interiors are replaced with the exterior dielectric. For circular cross section conductors, using the surface impedance of an isolated circular conductor in the EII-based SRM yields an excellent approximation from low to high frequency. This technique can also be easily applied to any lossy multi-conductor line structure using polygonal cross-section conductors by using an appropriate effective internal impedance model.

SIMIAN: A TWO DIMENSIONAL MULTI-CONDUCTOR INTERCONNECT SERIES IMPEDANCE CALCULATOR

SIMIAN (Surface Impedance Method for Interconnect Analysis) is a two dimensional frequency dependent series impedance extraction tool for interconnects and transmission lines using conductors of rectangular cross section based on the EII and SRM discussed above. Unlike the Volume Filament Method [19], only the surface of the conductor is divided, which can save significant amounts of computation time, especially when the cross sectional size of the conductor(s) is (are) comparable to the skin depth [14]. This method has also been extended to solve three dimensional problems [15]. SIMIAN returns the frequency dependent series impedance matrix for an n-conductor system, i.e., the n x n matrix consisting of self and mutual resistances and self and mutual inductances of and between all n conductors.

The SIMIAN program was successfully complied with ANSI C(g++). The platforms tested thus far include:

- Sparc 20 machine with Sunos 4.1.3
- Sparc 20 machine with Solaris 2.5
- Pentium machine with Linux
- HP workstation

The progran can be obtained over the World Wide Web at the url:

http://weewave.mer.utexas.edu/MED_files/MED_research/Intrcncts/SIMIAN_stuff/simian_links.html

Since the total number of ribbons used for each conductor determines the computation time, it is very important to reduce them without loss of accuracy. Since SIMIAN only divides the conductor on its surface, the problem can be reduced from N^2 to 4N compared to the volume filament method. However, more significant advantage comes from reduction of N itself. To get accurate result in the volume filament method, each segment has to be comparable in size to the skin depth at the frequency of interest; if a filament is much larger than about 1/3 of a skin depth, serious error can result. However, in the surface ribbon method a much smaller number of segments can be used while maintaining reasonable accuracy (typically less than 1% error at "low" frequencies, perhaps as much as 10% over a narrow band of frequencies at "mid" frequency, and again about 1% at "high" frequency). For most cases using more than five ribbons on each side would not be necessary, and in many cases as few as one per face is necessary.

Figure 5 shows minimum segmentation method [20] using '**plate**' option in Conductor type variable applied to ground plane. Only one ribbon is used on each side of signal line resulting in a total of 20 ribbons.

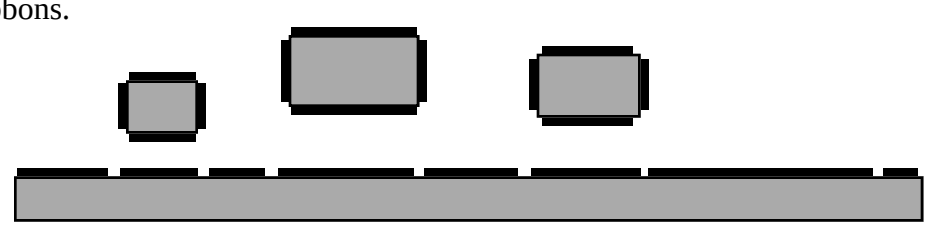

Figure 5: Minimum Segmentation Scheme with ground plane.

Examples and Results

Square Twin Lead

Example 1 is simulated with SIMIAN and compared with FastHenry [21] that uses the volume filament method accelerated using a multi-pole algorithm. As Fig. 6 shows, SIMIAN can reduce matrix size significantly. For the problem given, SIMIAN only uses 30 to 40 total ribbons while the volume filament method needs more than 800 filaments to accurately predict total resistance at high frequency. FastHenry accelerates matrix calculation with the help of a multi-pole algorithm, and this same algorithm can also be applied to the surface ribbon method. Figure 7 shows the results of FastHenry, SIMIAN, and the surface ribbon method (SRM) using a multi-pole algorithm. A total 40 ribbons were used for SIMIAN and SRM with multi-pole algorithm, while 800 filaments were used for FastHenry. In this particular example, the time advantage can be 400 to 8000 times faster than using the volume filament method, depending on what method is used for matrix calculation. Considering this is for only one frequency point, tremendous time savings can be achieved by using the SRM.

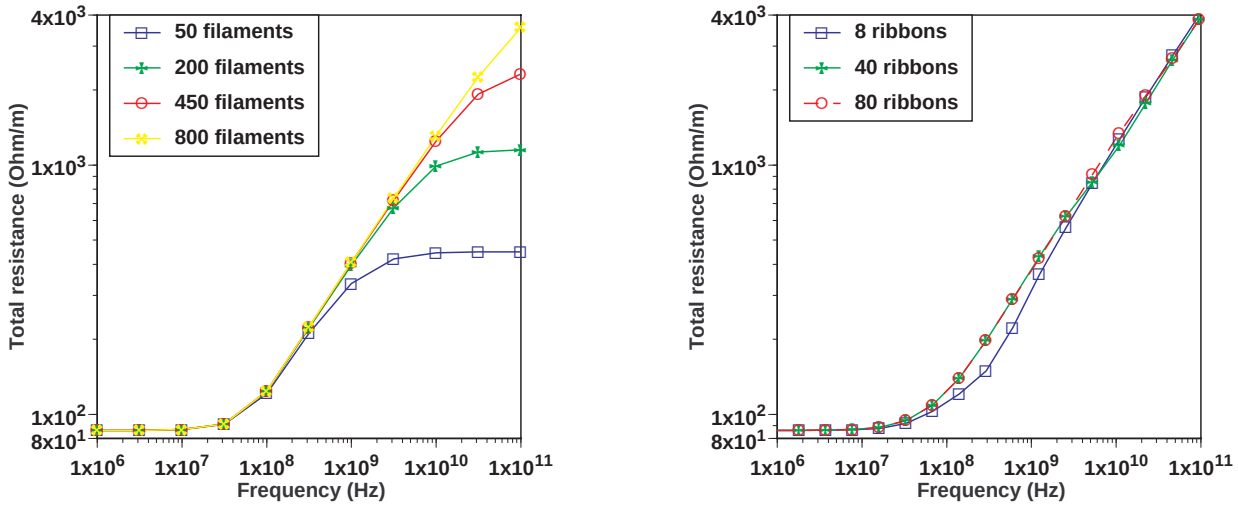

(a) (b)

Figure 6: (a) FastHenry [21] results versus number of filaments; (b) SIMIAN versus number of ribbons.

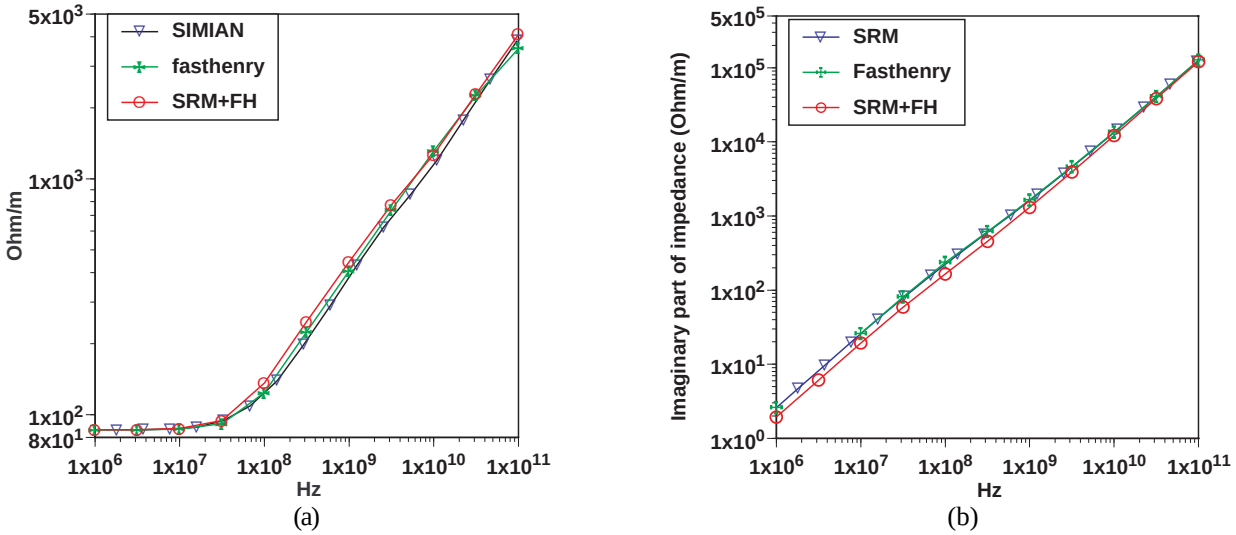

(a) (b)

Figure 7: solid line: SIMIAN (40 ribbons); circle: SRM with multi-pole algorithm (40 ribbons); cross: FastHenry (800 filaments). (a) Real part of total Impedance (R). (b) Imaginary part of total Impedance (ωL).

Three Conductors over Finite Size/Conductivity Ground Plane

Figure 8 shows results from simulating the three conductor problem shown below. The total number of ribbons used in SIMIAN was 20, which was considerably less than FastHenry (1250). Reasonable accuracy was achieved through SIMIAN within a second (20 frequency points with SPARC 20).

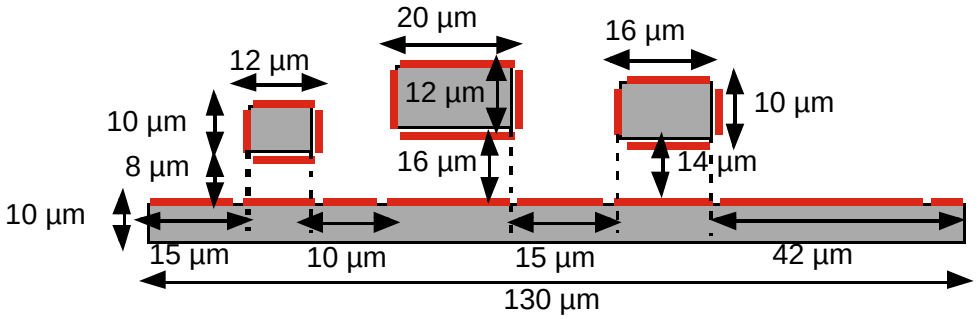

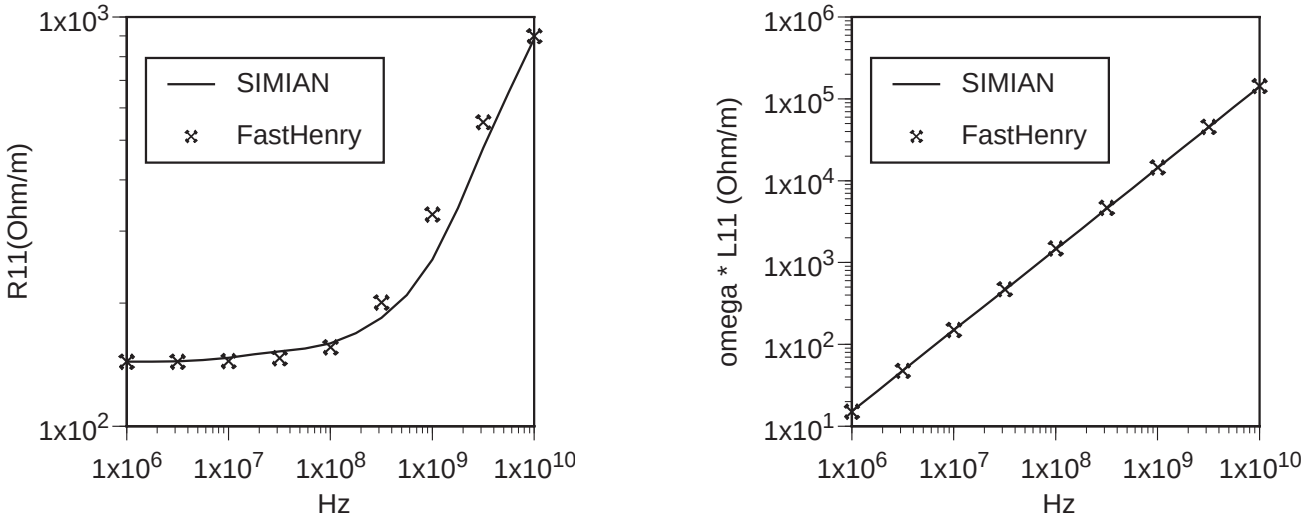

(a)Example 2, Z11

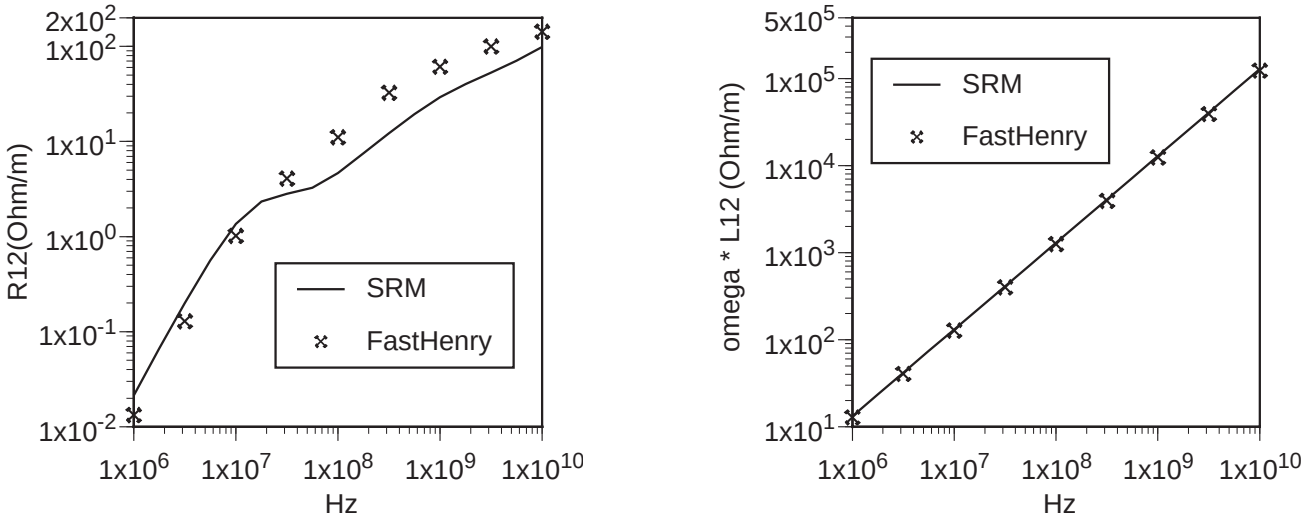

(b)Example 2, Z12

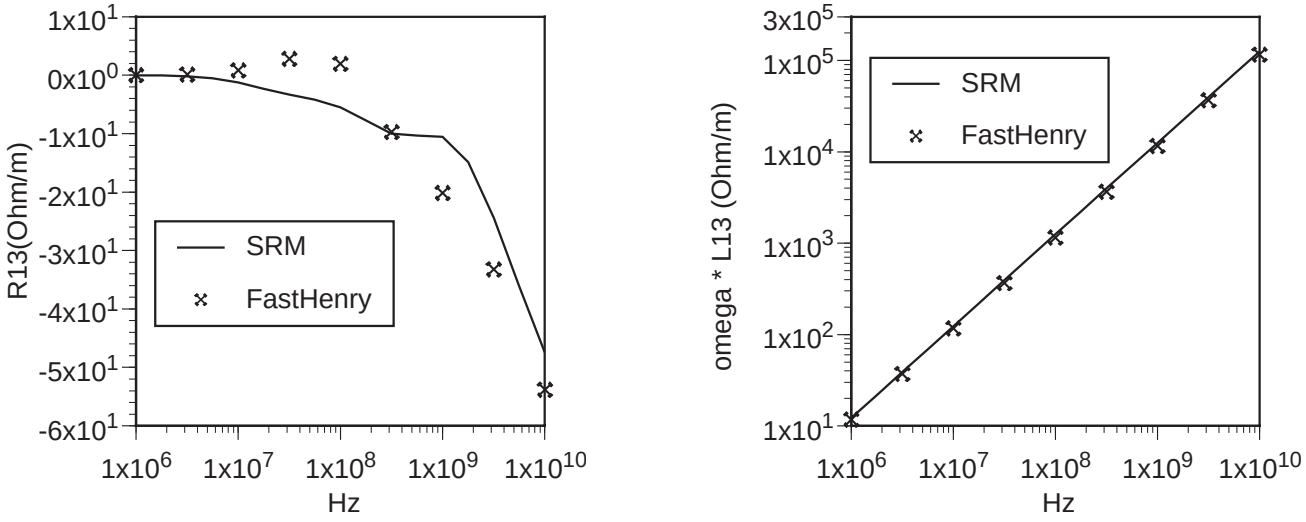

(c)Example 2, Z13

Figure 8: Real and Imaginary part of Series Impedance of Example 2.

EFFICIENT TIME DOMAIN BOUNDARY CONDITIONS FOR FINITE CONDUCTIVITY METALS

In the frequency domain, surface impedance boundary conditions (SIBCs) as discussed above have been used effectively to remove conductors from the solution space, thereby gaining computational speed. In the time domain, Tesche [22] has formulated a convolution-based time-domain integral equation that uses a transformation of frequency domain surface impedance into the time domain. Recently, attempts have been made to overcome these difficulties using Prony's method [23, 24] or Chebyshev approximation [25], which allows the transformation of frequency domain surface impedance into time domain exponentials. However, these procedures can be computationally arduous and the applications have been primarily limited to radiation problems where high frequency approximations (i.e., the surface impedance is a purely local quantity and equal to $1/\sigma\delta$) are sufficient for accurate results. Here we show how the EII model discussed above can be transformed into a very efficient time domain boundary condition for finite conductivity conductors.

Circuit Representation of the EII

In [14] the EII was used as a boundary condition to accelerate the volume filament method [19]. In this surface ribbon method (SRM), the EII is approximated using the surface impedance of an isolated conductor. Figure 9(a) shows how EII approximations for a rectangular conductor are calculated [26]. The EII of the half plate (Fig. 1a, **A**) is approximated using:

$$Z_A = \sqrt{\frac{j\omega\mu_o}{\sigma}} \Big/ W \tanh\left(\sqrt{j\omega\mu_o\sigma}\,\frac{T}{2}\right) \quad , \tag{18}$$

where W is the width of the ribbon and T is the thickness of the conductor. The EII of each triangle (Fig. 1a, **B**) is approximated using:

$$Z_B = \frac{\sqrt{-j\omega\mu_o\sigma}\,J_0\left(\sqrt{-j\omega\mu_o\sigma}\,H\right)}{\sigma W \cdot J_1\left(\sqrt{-j\omega\mu_o\sigma}\,H\right)} \quad , \tag{19}$$

where W is the base and H is the height of the iso-triangle.

For time domain calculation it would be advantageous to replace the frequency dependent equations for the EII approximations (eqs. 18 and 19) with frequency independent circuit models. In [27] a compact circuit model consisting of four resistors and three inductors (Fig. 9(b)) was used to accurately model the skin effect in circular conductors. The values of each element are related by the simple rules

$$\frac{R_i}{R_{i+1}} = RR \quad , \; i = 1, 2, 3. \qquad \frac{L_i}{L_{i+1}} = LL \quad , \; i = 1, 2 \quad , \tag{20}$$

where RR and LL are constants to be determined. Requiring the dc resistance and inductance of this circuit model to equal the value from eqs. 1 and 2 yields

$$RR^3 + RR^2 + RR + (1 - \alpha_R) = 0, \text{ with } \alpha_R = C_1 \frac{p}{\delta_{\max}} = \frac{R_1}{R_{dc}}, \; \delta_{\max} = \sqrt{\frac{2}{\omega_{\max}\mu_o\sigma}} \tag{21}$$

$$\left(\frac{1}{LL}\right)^2 + \left(1 + \frac{1}{RR}\right)^2 \frac{1}{LL} + \left(\left[\frac{1}{RR}\right]^2 + \frac{1}{RR} + 1\right)^2 - \alpha_L \left(\left[1 + \frac{1}{RR}\right]\left[\left\{\frac{1}{RR}\right\}^2 + 1\right]\right)^2 = 0 \; , \tag{22}$$

where $\alpha_L = C_2\alpha_R = L_{dc}/L_1$, $\omega_{\max}$ is highest frequency of interest in the input waveform, and p is the conductor depth parameter, e.g., the height of the iso-triangle, thickness of half plate $T/2$, or radius of a circle (for circular conductors). C_1 and C_2 are constants unique to the geometry of the conductor: (0.56, 0.315) for the iso-triangle; (10.8, 0.2) for the half plate; and (0.53, 0.315) for a circular conductor.

Using eqs. 20-22, the values of the circuit model can be determined for a given geometry conductor. In the s-domain, this model can be represented as

$$Z(s) = R_1 \frac{s^3 + a_2 s^2 + a_1 s + a_0}{s^3 + b_2 s^2 + b_1 s + b_0} \quad , \tag{23}$$

where eq. 23 is easily convertible to time domain exponential form. Figure 10 shows the accuracy of this model for a half plate. The accuracy for other geometries is presented in [27].

(a)

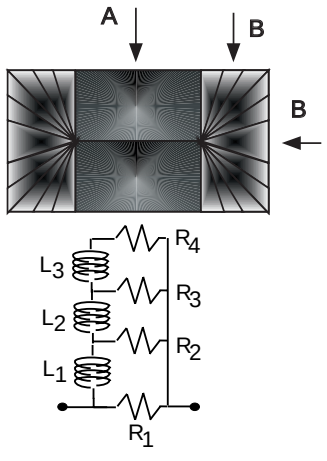

(b)

Figure 9: EII circuit for rectangular conductors.
(a) EII calculation of rectangular conductor; (b) Compact equivalent circuit model for the EII.

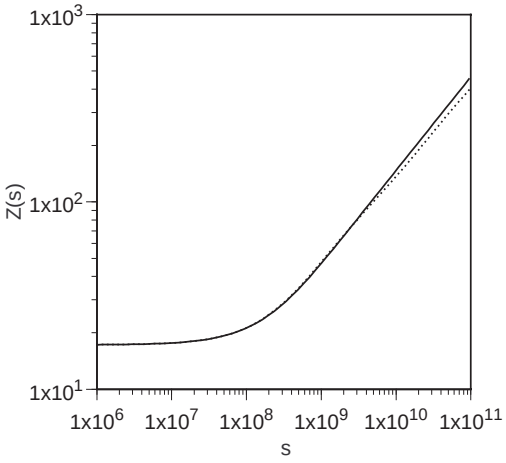

Figure 10: Surface impedance comparison in s-domain. solid line: eq. 1, dotted line: circuit representation. W=100 μm, T=20 μm.

Formulation of Multiconductor Transmission Line Equation

To formulate a transmission line equation, first one of the ribbons on the return conductor (ground conductor) is considered as a "ground ribbon" (labeled as the 0^{th} ribbon) and all the other ribbons are considered as signal ribbons. In the 2-dimensional frequency domain, the equation can be formulated as [14, 19]

$$[Z_{eii}][I] + j\omega[L][I] = \frac{\partial}{\partial z}[V] \tag{24}$$

Equation 24 is formulated under the assumption that all the currents are returned through the 0^{th} ribbon, and can be represented in the s-domain as

$$\frac{\partial}{\partial z}[V(s)] = [Z_{eii}(s)][I(s)] + s[L][I(s)] = \left[\frac{Z_{eii}}{s}\right] s[I(s)] + [L] s[I(s)] \quad . \tag{25}$$

Equation 25 can be transformed into the time domain as

$$\frac{\partial}{\partial z}[V(t)] = [\zeta(t)] * \frac{\partial}{\partial t}[I(t)] + [L]\frac{\partial}{\partial t}[I(t)] \quad , \tag{26}$$

where $[\zeta(t)]$ is inverse Laplace transform of $\left[\frac{Z_{eii}}{s}\right]$ (which is a rational function) and '*' is convolution. Using the circuit representation for the EII's given above $[\zeta(t)]$ can be easily converted into a sum of exponentials. In [23], the convolution is solved with an approximate recursive relationship

$$Y(n\Delta t) = X(n\Delta t) * \left(K \cdot e^{Pn\Delta t}\right) = K\Delta t + e^{P\Delta t} X\left((n-1)\Delta t\right) \tag{27}$$

Applying eq. 27 to eq. 26 results in

$$\frac{\partial}{\partial z}[V(t)] = [[L] + [K]][I(t)] + [V_{ds}(t)] = [L'][I(t)] + [V_{ds}(t)] \quad , \tag{28}$$

where $[V_{ds}(t)]$ is a dependent voltage source (per unit length) that depends on the poles of the EIIs and current values at the previous time, and $[L']$ is a matrix that depends on the residues of the EIIs and loop inductances of the ribbons. Note that $[L']$ is time independent, and so eq. 28 is very similar to the equation that results for a lossless transmission line. Another equation can be derived using Kirchoff's current law,

$$\frac{\partial}{\partial z}[I(t)] = [G][V(t)] + [C]\frac{\partial}{\partial t}[V(t)] \quad . \tag{29}$$

To verify the equations given here, an FDTD method [28] is applied to eqs. 28 and 29; this does require the inversion of $[L']$, but since $[L']$ is time independent, the inverse need be calculated only once. As an example problem Fig.11 shows the cross section of two, coupled, finite thickness microstrip lines over a finite width ground plane. All conductors (including the ground plane) have finite conductivity. Figure 12 compares the FDTD time domain calculation and FFT results using both the full dispersion curve and a simple R_{dc}-L-C transmission line model. Table 2 compares the computation times required for various methods. Due to the simplicity of the resulting equations, various pre-existing simulation techniques can be easily applied. FDTD result shows good agreement with FFT result, with substantially faster computation compared to even very efficient frequency domain calculations.

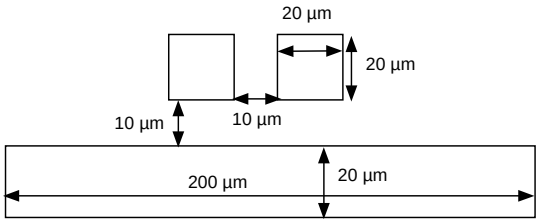

Figure 11: Cross section of coupled microstrip lines used as a test.

method	pre-calculation	main calculation (FDTD or FFT)
SRM-FDTD	0.5 sec	89.5 sec
SRM-FFT	149 sec	0.5 sec
FM-FFT	163,095 sec	0.5 sec

Table 2: Computation time comparison (Sparc 20 workstation).
SRM-FDTD: method used in this paper; SRM-FFT: Surface ribbon method [14] in frequency domain, then FFT applied; FM-FFT: Filament method [19, 21] in frequency domain, then FFT applied.

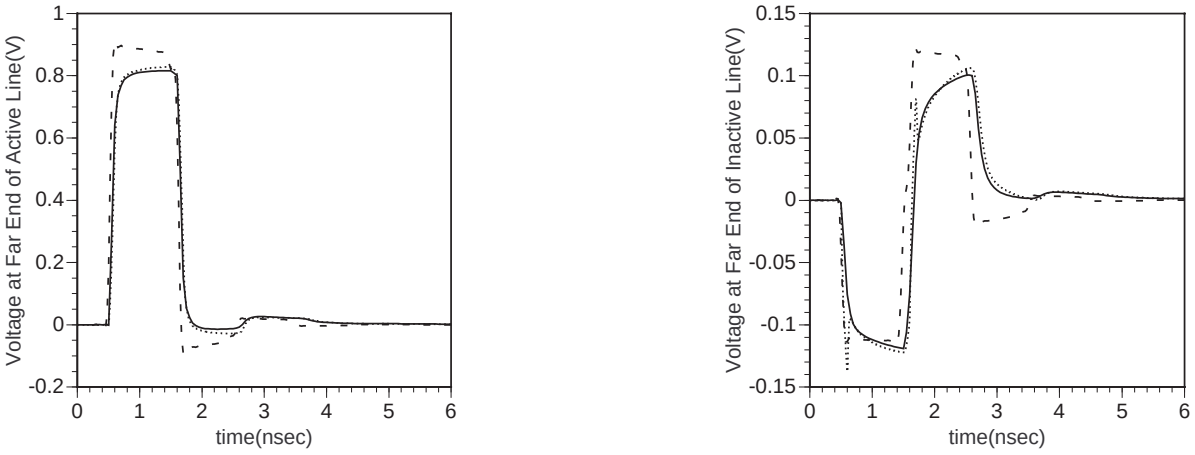

(4a) (4b)

Figure 12: Results for coupled miscrostrips over a finite ground plane.
Source resistance used was 5 , termination resistance 50 , line lengths 10 cm. (a) Far end response of the active line. (b) Far end response of the quite (victim) line. Solid line: FFT result; dotted line: FDTD technique in this paper; dashed line: R_{dc}-L-C circuit.

HP-FINITE ELEMENTS APPLIED TO ELECTROMAGNETIC PROBLEMS

Another important advance in the area of computational electromagnetics for application to mixed signal simulation has been in the area the finite element method (FEM). A new *hp*-adaptive technique has recently been validated that allows the local variation of both the element size (*h*) and the order of approximation (*p*). This approach has the advantage that complex structures should be easily simulated. The formulation has been demonstrated to allow discontinuous changes in material properties (such as the change from a dielectric to a metal), to be stable, and to easily handle curvilinear geometries. Extensive numerical testing is still required in this area.

EXPERIMENTAL MEASUREMENTS ON A PROTOTYPICAL PERSONAL COMMUNICATIONS SERVICES (PCS) SYSTEM

Our research activities in this area have been focused on building RF transceivers and baseband circuits for a handset testbed at 1.8GHz, the personal communication services(PCS) band. One important objective of this effort is to fully understand how the PCB layout, chip placement and packaging affect the overall wireless system specifications. This knowledge will help us to properly design multi-chip module (MCM) package for wireless communication systems.

The stability of frequency synthesizers, realized by phase locked loop, is critically important to the quality of wireless communications. If they lose lock even for a short period of time, they can cause significant problems with the modulation and demodulation. In our experiments, we found that the phase locked loop (PLL) was very sensitive to the interference from the power supply, sudden changes of impedance, and interference from power amplifiers. The RF transceivers we built were for the time-division-duplex (TDD) applications, in which the transceivers transmit in a 5ms slot and receive in another 5ms slot. During the transition period, the transmitter mixer is turned off and on to minimize the RF coupling between the transmit and receive parts. However, this causes sudden changes of the load impedance to the PLL and unlocks the PLL. Although the PLL can recover from this sudden change eventually, it may cause significant distortion or phase noise to the beginning part of the signal. Hence, in a mixed signal package, it is better to build some driver on the die or inside the package to avoid the detrimental effect due to the change of impedance. Also, the PLL must not share the same power supply as the power amplifier since the supply current surges after the power amplifier is turned on and dips if the power amplifier is turned off. This is another source for the PLL to lose lock for a short period of time. Hence, in the MCM package, we should have a different VCC pin just for the PLL power supply.

Another source of the PLL problem is due to the leakage power from the power amplifier. If we lay the RF board on a table, there is no problem. However, once we place another baseband board on the top of that, the leaked power will be reflected from the baseband board and coupled to the PLL. If we wish to package a PLL in the same MCM package as the power amplifier, care must be taken to isolate the PLL from the power amplifier.

On the baseband board, we used the Motorola digital signal processor MC56167 as a vocoder DSP. There are several delicate design issues and test issues we would like to address. This part is a mixed signal part. Although the analog ground and digital ground are separate in the chipset, care must be taken to eliminate the digital noise in the analog codec part. We have tried numerous PCB layouts and still could not eliminate the digital background noise. Later we managed to minimize the noise by balance the load of the DSP. In our vocoder, the encoding part takes much more time than the decoder part. Thus, the DSP may be busy for some time and idle for some time. In this case, the noise from the DSP shows some periodical pattern and is more easily sensed by a human ear. We managed to change the DSP structure and made it busy all the time. This makes the noise white and not so sensible. Therefore, for testing the digital interference to the analog circuits in a mixed signal package, we should try to have several test patterns with different loading to assess the digital interference to the analog part.

SUMMARY AND FUTURE PLANS

In summary, for the period 9/1/96 through 9/1/97, we have extended our ability to efficiently simulate the behavior of realistic interconnects that make use of finite conductivity metals. In particular, we have developed and tested:

- a fundamental electromagnetic formulation of the effecive internal impedance boundary condition for finite conductivity metals.
- an extremely efficient multi-conductor simulation program using the surface ribbon method for interconnect series imepdance calculations.
- initial computational electromagnetics code for FEM simulations.
- experimental work on mixed signal PCS prototypes to investigate analog system corruption due to cross talk and power supply noise.

Work is on-going in all these areas. Future effort in simulations will be focused on time domain simulation, in particular the development of efficient conductor boundary conditions for use in the method of characteristics, that has better stability behavior than the FDTD method.

PUBLICATIONS SUPPORTED IN WHOLE OR IN PART BY THIS GRANT DURING THIS REPORTING PERIOD:

Beom-Taek Lee, Sangwoo Kim, Emre Tuncer, and Dean P. Neikirk, "Effective Internal Impedance Method for Series Impedance Calculations of Lossy Transmission Lines: Comparison to Standard Impedance Boundary Condition," submitted to: IEEE Transactions on Microwave Theory and Techniques, June 1997.

Sangwoo Kim and Dean P. Neikirk, "Time Domain Multiconductor Transmission Line Analysis Using Effective Internal Impedance," *IEEE 6th Topical Meeting on Electrical Performance of Electronic Packaging*, San Jose, CA, October 27 - 29, 1997, pp.

REFERENCES

[1] J. Jin, *The Finite Element Method in Electromagnetics*: John Wiley & Sons, Inc., 1993.
[2] A. Darcherif, A. Raizer, J. Sakellaris, and G. Meunier, "On the use of the surface impedance boundary concept in shielded and multiconductor cable characterization by the finite element method," *IEEE Trans. Magnetics*, vol. 28, pp. 1446-1449, 1992.
[3] T. H. Fawzi, M. T. Ahmed, and P. E. Burke, "On the use of impedance boundary conditions in eddy current problems," *IEEE Trans. Magnetics*, vol. MAG-21, pp. 1835-1840, 1985.
[4] E. M. Deely, "Avoiding surface impedance modification in BE methods by singularity-free representations," *IEEE Trans. Magnetics*, vol. 28, pp. 2814-1816, 1992.
[5] J. R. Mosig, "Arbitrary shaped microstrip structures and their analysis with a mixed potential integral equation," *IEEE Trans. Microwave Theory Tech.*, vol. 36, pp. 314-323, 1988.
[6] B. J. Rubin, "An electromagnetic approach for modeling high-performance computer packages," *IBM J. Res. Develop.*, vol. 34, pp. 585-600, 1990.
[7] J. G. Maloney and G. S. Smith, "The use of surface impedance concepts in the finite-difference time-domain method," *IEEE Trans. Antennas Prop.*, vol. 40, pp. 39-48, 1992.
[8] J. H. Beggs, R. J. Luebbers, K. S. Yee, and K. S. Kunz, "Finite-difference time-domain implementation of surface boundary conditions," *IEEE Trans. Antennas Prop.*, vol. 40, pp. 49-56, 1992.
[9] M. A. Leontovich, "On the approximate boundary conditions for electromagnetic fields on the surface of well conducting bodies," *Investigations of Propagation of Radio Waves*, vol. B. A. Vvdensky, Ed. Moscow: Academy of Sciences USSR, pp. 5-20, 1948.
[10] D. J. Hoppe and Y. Rahmat-Samii, *Impedance Boundary Conditions in Electromagnetics*: A SUMMA Book, 1995.
[11] S. A. Schelkunoff, "The electromagnetic theory of coaxial transmission lines and cylindrical shields," *Bell System Technical Journal*, vol. 13, pp. 532-579, 1934.
[12] T. B. Senior, "Impedance boundary conditions for imperfectly conducting surfaces," *Applied Science Research*, vol. 8, pp. 418-436, 1960.
[13] K. M. Mitzner, "An integral equation approach to scattering from a body of finite conductivity," *Radio Science*, vol. 2, pp. 1459-1470, 1967.
[14] E. Tuncer, B.-T. Lee, and D. P. Neikirk, "Interconnect Series Impedance Determination Using a Surface Ribbon Method," IEEE 3rd Topical Meeting on Electrical Performance of Electronic Packaging, Monterey, CA, Nov. 2-4, 1994, pp. 249-252.
[15] B.-T. Lee, E. Tuncer, and D. P. Neikirk, "Efficient 3-D Series Impedance Extraction using Effective Internal Impedance," IEEE 4th Topical Meeting on Electrical Performance of Electronic Packaging, Portland, OR, Oct. 2-4, 1995, pp. 220-222.
[16] B.-T. Lee and D. P. Neikirk, "Minimum Segmentation in the Surface Ribbon Method for Series Impedance Calculations of Microstrip Lines," IEEE 5th Topical Meeting on Electrical Performance of Electronic Packaging, Napa, CA, October 28-30, 1996, pp. 233-235.

[17] A. K. Agrawal, H. L. Price, and S. H. Gurbaxani, "Transient Response of Multiconductor Transmission Lines Excited by a Nonuniform Electromagnetic Field," *IEEE Transactions on Electromagnetic Compatibility*, vol. EMC-22, pp. 119-129, 1980.
[18] S. Ramo, J. R. Whinnery, and T. V. Duzer, *Fields and Waves in Communication Electronics*, 2nd ed. New York: Wiley, 1984.
[19] W. T. Weeks, L. L. Wu, M. F. McAllister, and A. Singh, "Resistive and inductive skin effect in rectangular conductors," *IBM Journal of Research and Development*, vol. 23, pp. 652-660, 1979.
[20] B.-T. Lee and D. P. Neikirk, "Minimum Segmentation in the Surface Ribbon Method for Series Impedance Calculations of Microstrip Lines," IEEE 5th Topical Meeting on Electrical Performance of Electronic Packaging, Napa, CA, October 28-30, 1996, pp. 233-235.
[21] M. Kamon, M. J. Tsuk, and J. White, "FASTHENRY: A Multipole-Accelerated 3-D Inductance Extraction Program," *IEEE Transactions on Microwave Theory and Techniques*, vol. 42, pp. 1750-1758, 1994.
[22] F. M. Tesche, "On the Inclusion of Loss in Time-Domain Solutions of Electromagnetic Interaction Problems," *IEEE Trans. on Electromagnetic Compatibility*, vol. 32, pp. 1-4, 1990.
[23] S. Kellali and B. Jecko, "Implementation of a Surface Impedance Formalism at Oblique Incidence in FDTD Method," *IEEE Trans. on Electromagnetic Compatibility*, vol. 35, pp. 347-355, 1993.
[24] J. G. Maloney and G. S. Smith, "The Use of Surface Impedance Concepts in the Finite-Difference Time-Domain Method," *IEEE Trans. on Antennas and Propagation*, vol. 40, pp. 38-48, 1992.
[25] K. S. Oh and J. E. Schutt-Aine, "An Efficient Implementation of Surface Impedance Boundary Conditions for the Finite-Difference Time-Domain Method," *IEEE Trans. on Antennas and Propagation*, vol. 43, pp. 660-666, 1995.
[26] E. Tuncer and D. P. Neikirk, "Efficient Calculation of Surface Impedance for Rectangular Conductors," *Electronics Letters*, vol. 29, pp. 2127-2128, 1993.
[27] S. Kim and D. P. Neikirk, "Compact Equivalent Circuit Model for the Skin Effect," IEEE International Microwave Symposium, Vol. 3, San Fransisco, CA, 1996, pp. 1815-1818.
[28] C. R. Paul, "Incorporation of Terminal Constraints in the FDTD Analysis of Transmission Lines," *IEEE Trans. on Electromagnetic Compatibility*, vol. 36, pp. 85-91, 1994.